DELTA-K WIDEBAND SAR INTERFEROMETRY FOR DEM GENERATION AND PERSISTENT SCATTERERS USING TERRASAR-X

Ramon Brcic, Michael Eineder, Richard Bamler, Ulrich Steinbrecher, Daniel Schulze, Robert Metzig, Konstantinos Papathanassiou[(1)], Thomas Nagler, Florian Mueller[(2)], Martin Suess[(3)]

[(1)] German Aerospace Center, DLR, Muenchnerstr. 20, 82234 Wessling, Germany,
Email: {Ramon.Brcic, Michael.Eineder, Richard.Bamler, Ulrich.Steinbrecher, Daniel.Schulze, Robert.Metzig, Kostas.Papathanassiou}@dlr.de
[(2)] ENVEO IT GmbH, ICT - Technologiepark, Technikerstrasse 21a, A-6020 Innsbruck, Austria,
Email: {Thomas.Nagler, Florian.Mueller}@enveo.at
[(3)] ESA, Keplerlaan 1, 2200 AG Noordwijk, Netherlands, Email: Martin.Suess@esa.int

ABSTRACT

Wideband SAR systems such as TerraSAR-X allow estimation of the absolute interferometric phase without resorting to error prone phase unwrapping. This is achieved through the delta-k technique that exploits frequency diversity within the range bandwidth to simulate a SAR system with a much longer carrier wavelength. This benefits all interferometric applications including DEM generation and land surface motion determination. Here we present the results of an ESA study (21318/07/NL/HE) into using delta-k absolute phase estimation for DEM generation and PSI (Persistent Scatterer Interferometry). Using TerraSAR-X data, examples from a delta-k DEM generation system are shown which avoid the errors induced by conventional phase unwrapping. For PSI, the possibilities of absolute phase estimation for a single PS are explored in theory and examples where wideband estimation is compared to conventional PSI processing for a stack of acquisitions over Paris.

1. INTRODUCTION

Determining the number of integer phase cycles has been a problem since the first SAR interferograms were formed. For DEM (Digital Elevation Model) generation, this problem is solved by PU (Phase Unwrapping) [3] where the gradients between interferogram pixels are integrated to achieve phase differences larger than one cycle. For PSI (Persistent Scatterer Interferometry) [4][5], the absolute velocity and height difference between two points are determined by a time series analysis involving 2-dimensional frequency estimation. Both methods are prone to errors if the gradients are aliased, i.e. larger than the spatial or temporal sampling intervals allow for. All mentioned applications would enormously profit from a gradient independent means to estimate the absolute phase between pixels.

We concentrate on the delta-k method [6] which uses frequency diversity within the range bandwidth to resolve for the unknown integer phase cycle. The optimal estimator determines the residual shift between the two SAR images by complex cross correlation and highly accurate peak determination with subpixel accuracy [1]. Delta-k estimates this shift in a computationally efficient sense by splitting the SAR images into subbands and determining the phase-frequency gradient between the subband interferograms. This simulates a SAR system with a much longer carrier wavelength than the actual one, increasing the HoA (Height of Ambiguity) to a point where PU is unnecessary. Other methods use multiple SAR images with different frequencies or geometries [7]–[12].

We show that for DEM generation, delta-k can be used as a standalone method or to support/validate PU. The trade-off in this case is that the large HoA afforded by delta-k is accompanied by reduced resolution. For PSI we investigate delta-k absolute phase estimation for a single PS from both a theoretical perspective and through experiments. In both cases delta-k provides independent estimates for either a patch in DEM generation or a single pixel in PSI and this eliminates the main disadvantage of conventional techniques – that a single PU error can propagate and affect large areas.

2. DELTA-K ABSOLUTE PHASE ESTIMATION

The theory of delta-k absolute phase estimation and its practical application are detailed in [1][2][6] and only a brief summary is given here.

For repeat-pass interferometry the relationship between interferometric phase, ϕ, and differential range, Δr, is

$$\phi = 4\pi \frac{f_C}{c} \Delta r \,, \tag{1}$$

where f_C is the radar carrier frequency and c the speed of light. Taking the differential phase between two subband interferograms with range bandwidths b and range centre frequencies $f_C \pm f_0$, as illustrated in Figure 1, gives the delta-k phase,

$$\Delta\phi = \phi_2 - \phi_1 = 4\pi \frac{2 f_0}{c} \Delta r \,. \tag{2}$$

The delta-k phase can then be interpreted as the interferometric phase at a simulated carrier frequency $2f_0 << f_C$, i.e. at a much longer wavelength than the actual carrier. Consequently, the HoA of the delta-k phase is

Proc. 'Fringe 2009 Workshop', Frascati, Italy,
30 November – 4 December 2009 (ESA SP-677, March 2010)

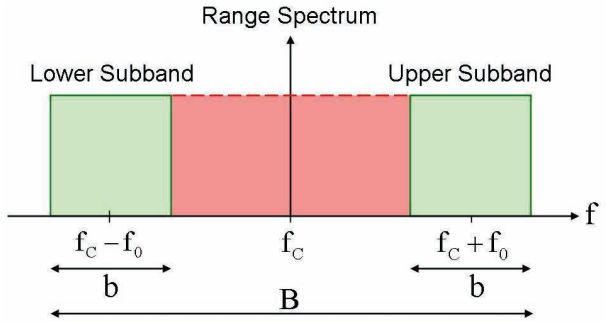

Figure 1. Bandpass filtering of the fullband images to obtain the subband images.

increased by the delta-k scaling factor $k_\Delta = f_C/2f_0$ relative to the fullband interferometric phase. For standard TerraSAR-X acquisitions with range bandwidth B = 150 MHz, k_Δ=64. Delta-k HoAs on the order of 1 km are then typical. Such a large HoA makes PU trivial or even unnecessary. The delta-k absolute phase estimate at the carrier frequency is obtained by scaling the delta-k phase up by k_Δ.

The optimal choice of subbands, $b=B/3$, $f_0=B/3$, achieves the maximum Fisher efficiency of 0.89, meaning the theoretical standard deviation of the delta-k absolute phase estimate is 6% greater than the theoretical minimum obtained by complex correlation. While an extension of two subband delta-k to multiple subbands achieves higher efficiencies, the performance improvement does not justify the increased complexity.

3. WIDEBAND DEM GENERATION

The delta-k algorithm for DEM generation was considered in detail in [2]. The major consideration is that the standard deviation of the delta-k absolute phase estimate at the carrier frequency is greater than the standard deviation of the subband interferometric phase by a factor $\approx\sqrt{2}k_\Delta$. For an accurate height estimate this must be compensated for and hence the delta-k phase must be smoothed prior to scaling. Delta-k is then a trade-off between resolution and the ability to resolve phase ambiguities due to the increase in HoA.

Figure 2 compares rewrapped absolute phase estimates from conventional MCF (Minimum Cost Flow) PU and delta-k for B=100 MHz stripmap acquisitions over the salt lake Salar de Arizaro in Argentina. The HoA at the carrier frequency was 7.4 m/cycle – using b=33 MHz subbands for delta-k processing increased this by the factor k_Δ=145 to 1076 m/cycle. The above mentioned increase in height estimation error is compensated for by smoothing the delta-k phase over 2000 independent samples giving a resolution of ~180×300 m (slant range × azimuth) compared to the fullband interferometric resolution of 10×17 m using 36 looks.

The fringe pattern for both estimates is very similar over the salt sea where the lack of topography and high coherence made unwrapping errors unlikely. The

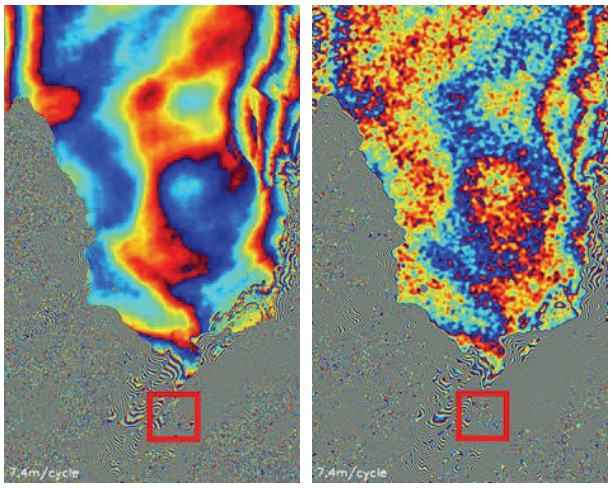

Figure 2. (Left) Fullband interferogram MCF PU estimate of the absolute phase. (Right) Delta-k estimate of the absolute phase. The red box denotes the lava tongue feature.

pattern over the extremely flat salt sea is largely caused by atmospheric effects such as water vapour that affects standard and delta-k interferometry equally – see estimation of atmospheric effects in Section 3.2. In the mountainous area, which climbs up to ~2 km above the salt sea, phase errors do occur. A comparison with an SRTM DEM showed that MCF PU produced significantly more errors of a much larger magnitude than delta-k. A case in point is the lava tongue feature located within the red box in Figure 2.

The close-up in Figure 3 shows how this region is surrounded by phase errors that essentially disconnect it from the rest of the interferogram making PU extremely difficult. The estimated height profile along a transect through the middle of this region also shown in Figure 3 confirms that conventional MCF PU fails, whereas the delta-k solution compares well with that from the correct SRTM C-band DEM.

Further experiments [2] demonstrate delta-k at higher bandwidths and using the custom split bandwidth chirp acquisitions described in Section 3.1. This shows that delta-k is well suited for PU control, i.e. as a standalone method against which the conventional estimate can be checked. For the upcoming TanDEM-X mission, delta-k will be used in the multibaseline PU as an a priori DEM.

3.1. Custom Split Bandwidth Chirps with TerraSAR-X

Transmitting a custom split bandwidth chirp that concentrates all energy into the subbands increases the SNR by a factor B/(2b) in comparison to a nominal chirp as no energy is lost through bandpass filtering to obtain the subbands [1]. During this study, such a custom split bandwidth waveform was developed, uplinked to TSX-1 and used for SAR imaging for the first time – we are not aware of another experiment

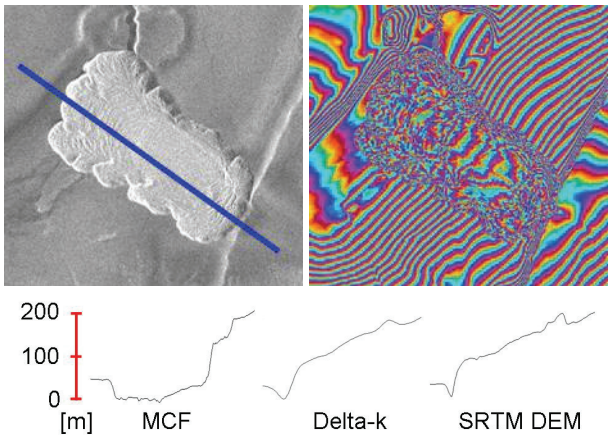

Figure 3. At top, a close-up of the lava tongue from Figure 2 for the (Left) SAR image and (Right) fullband interferometric phase. At bottom, the height profile of the transect shown in blue from (Left) MCF PU, (Middle) Delta-k and (Right) SRTM C-band DEM (0 m corresponds to elevation ~3600 m).

having used this technique before. This required special commanding with the satellite in experimental mode in order to upload the custom split bandwidth chirps.

Figure 4 shows the baseband spectrogram of such a custom split bandwidth chirp obtained from a transmit calibration pulse. The split bandwidth chirp, coloured red, consists of two down chirps with the same chirp rate, duration and bandwidth (b=37.5 MHz) but different centre frequencies and start/stop times. The upper subband chirp (150 to 112.5 MHz) is sent during the first half of the transmit pulse and the lower (−112.5 to −150 MHz) during the second half. This gave B/b=8 for a 6.0 dB increase in SNR.

Interference consisting of other chirps are visible in the spectrogram coloured blue at a greatly reduced power of

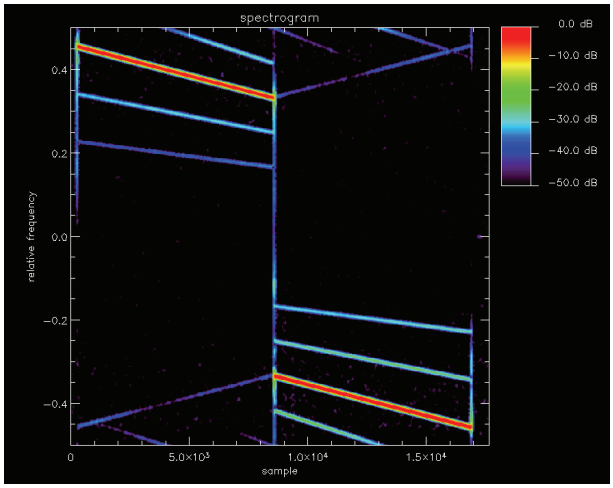

Figure 4. Baseband spectrogram of a TSX-1 transmit calibration pulse for a custom split bandwidth chirp acquisition. Range bandwidth 300 MHz, range sampling frequency 330 MHz, carrier frequency 9.65 GHz, subband range bandwidth 37.5 MHz.

30–40 dB below the custom chirp. They arise due to slight differences in the offset and gain of the in-phase and quadrature ADCs, nonlinearities in the hardware which cause harmonics and mirror frequencies.

See [2] for a processing example using custom split bandwidth chirp acquisitions.

3.2. Atmospheric Effects

Water vapour is the major contributor to spatial variability in the atmospheric path delay [13]. Its effect on the interferometric phase can be simulated given water vapour content maps at the master and slave acquisition times and knowledge of the acquisition geometry. Maps of atmospheric water vapour content were obtained from optical satellite data as provided by MODIS (Moderate Resolution Imaging Spectrometer) onboard the TERRA and ACQUA satellites.

Figure 5 shows an example of the simulated interferometric phase shift due to the atmosphere compared to the topography corrected interferogram – after removal of the topographic phase from the interferogram, what remains should be attributable to atmospheric delay. The example is for TerraSAR-X acquisitions taken on 12.08.2007 and 14.09.2007 over the salt sea Salar de Uyuni in Bolivia. The south-west (bottom-left) corner of the scene is a mountainous region while the flat salt sea covers the remainder. It should be noted that the MODIS acquisitions were taken at 15:00 UTC and the TerraSAR-X acquisitions at 22:54 UTC. The atmospheric structure certainly changed during these ~8 hours and hence only a qualitative comparison between the simulated shift and the topography corrected interferogram is possible. A qualitative comparison shows a similar pattern in the magnitude of the phase gradients. Any shift and rotation has to be attributed to the difference in acquisition times

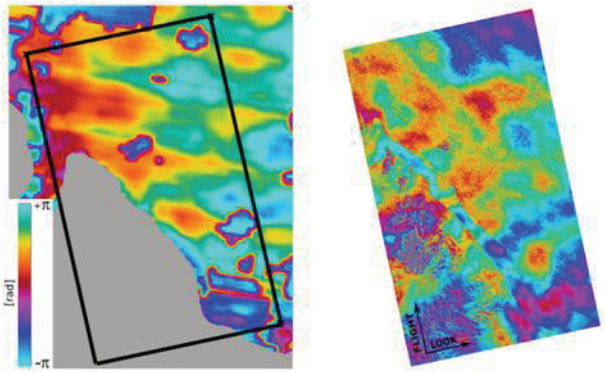

Figure 5. Estimation of atmospheric effects over Salar de Uyuni. (Left) Simulated interferometric phase shift due to atmospheric water vapour as derived from MODIS water vapour maps acquired at 15:00 UTC. Mountainous areas where the MODIS data was unreliable are shaded grey. The black box bounds the extent of the TerraSAR-X scene. (Right) TerraSAR-X topography corrected interferometric phase from TerraSAR-X data acquired at 22:52 UTC.

of the MODIS and TerraSAR-X data. Similar results were obtained for other acquisitions of this testsite. The effect of the hydrostatic component of the atmosphere (N_2, O_2, CO_2), which is mostly dependent on pressure and temperature and amounts to several fringes at X-band, shows little spatial variability over a scene and can be approximated as a constant interferometric phase shift. The effect of liquid water due to clouds is usually small compared to the hydrostatic and water vapour components and can be neglected [13].

4. WIDEBAND PERSISTENT SCATTERER INTERFEROMETRY

PSI (Persistent Scatterer Interferometry) is used to very accurately estimate not only the height but also the movement of a single PS. In order to extract the topographic and deformation parameters at the expected SCR (Signal to Clutter Ratio) of approximately 2 – 15 dB, hundreds or thousands of PSs must be combined in a network over a stack of interferograms from which the parameters are jointly estimated using LS (Least Squares) techniques, i.e. spatial PU.

The joint estimation required to perform the highly accurate spatial PU has some inherent limitations which delta-k techniques could overcome. A *sparse network of PSs is unwrapped over a time series of interferograms*, hence estimation of the absolute phase of a single PS in a single interferogram independent of other PSs and interferograms is not possible. Delta-k techniques allow estimation of the *absolute phase for a single PS in a single interferogram independent of other PSs and interferograms*. This requires, of course, PSs with sufficient SCR to avoid phase errors. The delta-k estimate would then contain the absolute phase components of displacement, atmosphere and topography. Given a stack of interferograms and a parametric model for the deformation, the topographic and deformation parameters could be estimated for a single PS. This would make it possible to at least control non-robust and time consuming PSI processing steps such as the periodogram or lambda-method.

4.1. Theoretical Performance Analysis

The optimal shift estimator that attains the Cramér-Rao Bound is the difference between shift estimates obtained from a complex cross-correlation in range between the master and slave SAR images and the sinc response of an ideal PS [1]. The variance of the corresponding complex cross-correlation absolute phase estimate is

$$\mathrm{Var}\,\hat{\phi}_{ABS} = \frac{3}{\pi^2}\left(\frac{f_C}{B}\right)^2 \frac{1}{SCR}\ [\mathrm{cycles}^2], \qquad (3)$$

where SCR is the Signal to Clutter Ratio. Note that in PSI, the contribution of clutter is expected to dominate that of the thermal noise in determining performance and so SCNR (Signal to Clutter plus Noise Ratio) ≈ SCR. The cross-correlation estimate has the same slant range resolution as the SSCs (Single look Slant range Complex image).

The variance of the delta-k absolute phase estimate for a PS can be shown to be

$$\mathrm{Var}\,\hat{\phi}_{ABS} = \frac{1}{2\pi^2}\left(\frac{f_C}{B}\right)^2 \frac{1}{\left(1-\tilde{b}\right)^2}\frac{1}{SCNR}\ [\mathrm{cycles}^2], \quad (4)$$

where SCNR refers to the subband value and $\tilde{b} = b/B$. For the case of a single PS surrounded by clutter in its and in neighbouring resolution cells, the subband SCR will be reduced by a factor $\tilde{b}$ compared to the fullband SCR. The SNR remains unchanged. The slant range resolution is reduced to that of the subband SSCs, a factor $\tilde{b}$ of that of the fullband SSC.

The efficiency of the delta-k estimator for PSs versus subband bandwidth is the same as that for distributed scatterers and hence the optimal subband bandwidth remains $b = B/3$ or $\tilde{b} = 1/3$ giving a maximum efficiency of 0.89 [1].

Figure 6 shows the standard deviation of the delta-k absolute phase estimate versus subband SCNR. At SCNR ≈ 33 dB the probability of a gross phase error ≥ 0.5 cycles is ≈ 5%. This can be taken as a threshold SCNR required for application of the delta-k method to a single PS. Below this threshold a gross phase error becomes increasingly likely, reaching 65% at SCNR=20 dB.

Several possibilities exist to improve the performance of wideband PSI. *Temporal averaging* over a stack of interferograms just as in standard PSI is one way and this is considered later. *Spatial averaging*, as was performed for DEM generation with distributed scatterers, defeats the purpose of PSI where the focus is on single PSs. System changes include use of a custom chirp, reducing the system noise figure and increasing the bandwidth. An *increase in bandwidth* and hence resolution reduces clutter due to the smaller range resolution cell size. Holding all other factors constant, the SCR will then increase in direct proportion to the bandwidth. Although the SNR will also decrease in direct proportion to the bandwidth due to increased thermal noise, this is not expected to make a significant difference for PSI because the effect of clutter outweighs that of thermal noise. For this reason, an increase in SNR brought about by reducing the system noise figure is also unlikely to significantly alter performance. The improvement brought about due to an increased SCR through increased bandwidth should continue until the attendant reduction in SNR is large enough such that thermal noise becomes the dominant noise source. As will be shown later, the SCR and SNR are separated by tens of decibels, implying a large

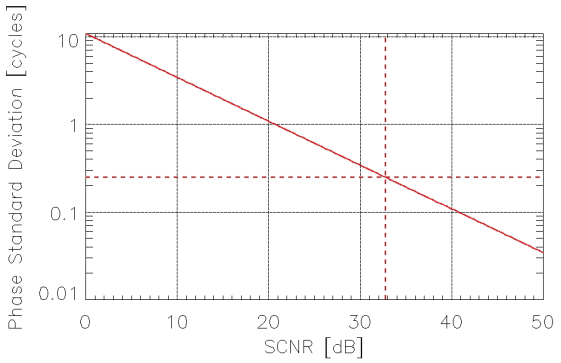

Figure 6. Standard deviation of the delta-k absolute phase estimate at the carrier frequency for a single PS using one interferogram versus subband SCNR. A standard deviation of ¼ cycles (horizontal dashed red line) corresponds to a phase error probability ≈ 5%, this occurs at SCNR ≈ 33 dB (vertical dashed red line). Example for carrier frequency 9.65 GHz, range bandwidth 300 MHz, subband bandwidth 100 MHz.

potential for improvement through increased bandwidth. Use of split bandwidth *custom chirps* where the energy is concentrated at the edges of the range bandwidth B is unlikely to help. The increase in subband energy raises the returned energy from both the PS and clutter equally leading to no change in SCR. While the SNR also rises, this is not significant in PSI for reasons already discussed above.

4.2. Delta-k Processing for PSI

The delta-k phase is computed in nearly the same way as for DEM generation. The major change is that a lower and upper subband *stack of acquisitions* are independently coregistered to a common master during InSAR processing. Minor changes between InSAR processing for PSI and DEM generation are 1) no spectral shift filtering and 2) outputs are fine coregistered subband stacks instead of the multilooked subband interferometric phase. Delta-k processing takes these fine coregistered subband stacks, computes the single look subband interferograms, corrects for FEP (Flat Earth Phase) and then computes the delta-k phase from a differential interferogram between the lower and upper subband interferograms. No smoothing or MCF PU is performed. This gives delta-k phase estimates for each interferogram. Scaling to the carrier frequency is performed implicitly by the *single delta-k interferogram* and *LS delta-k* height estimators, described later.

4.3. Results

Interferometric Stack Description

A stack of 25 B=300 MHz high resolution spotlight images of Paris was acquired over 16 months. The SSC pixel spacing was 0.45/0.79×0.85 m (slant/ground range × azimuth) with resolution 0.59/1.0×1.1 m. For conventional and delta-k PSI processing the SSCs were oversampled by a factor of two in range and azimuth. A baseline plot is shown in Figure 7. For InSAR stacking the common master was chosen to lie near the temporal centre of the stack. This gave normal baselines of 6–375 m. Figure 7 also shows that the HoAs lie mostly between 10–100 m at the carrier frequency and 0.5–5 km at the delta-k frequency. The large increase in the delta-k HoA corresponds to the delta-k scaling factor of k_Δ=48.25 when using the optimal subband bandwidth of b=100 MHz. We have concentrated on a small RoI (Region-of-Interest) around the Eiffel tower with dimensions 550×210 m on the ground.

Detection of Persistent Scatterers

Many strong scatterers are expected on the large metal structure of the Eiffel tower. Estimates of the SNR and SCR over the RoI are shown in Figure 8. The SNR was calculated from the calibrated amplitude images and the noise information in the TSX L1b product annotation parameter file. The SCR was estimated using GENESIS-PSI which determines clutter power by assessing both spatial and temporal statistics of the stack of SSCs. SNR can be calculated per SSC – Figure 8 is representative – while SCR can only be calculated from a stack of SSCs. The Eiffel tower clearly stands out with SNR values 20–50 dB and SCR values 0–30 dB –

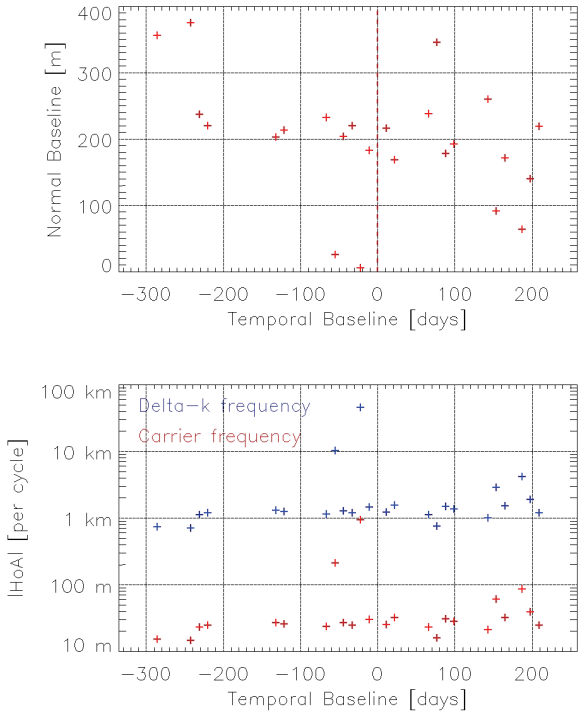

Figure 7. (Top) Normal baseline distribution for Paris stack. (Bottom) HoA at the carrier and delta-k frequencies.

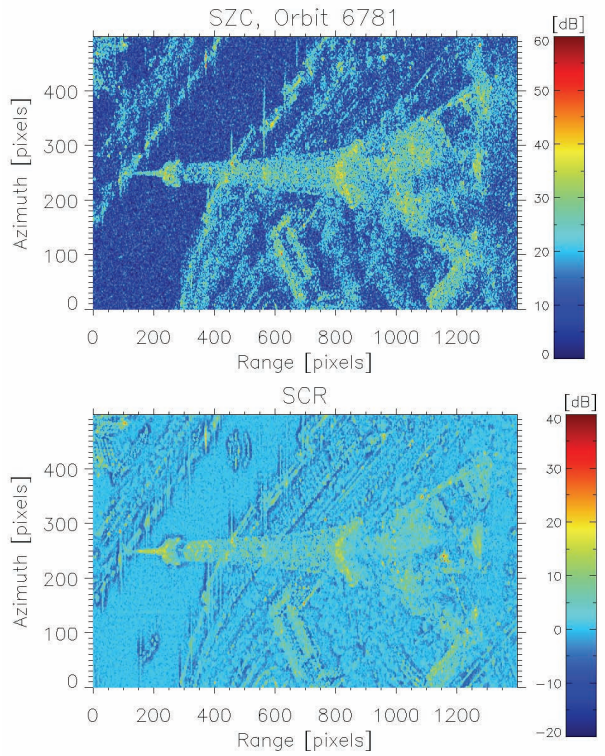

Figure 8. (Top) SNR over the RoI for the master orbit. (Bottom) SCR over the RoI.

showing that SNR and SCR are separated by 30 dB. There are approximately 10^4 pixels in the RoI with an SNR of at least 33 dB but very few with an SCR greater than even 20 dB. From these results, it appears that delta-k absolute phase estimation can only be applied to a select set of PSs.

The most suitable ~1700 PSs within the RoI are shown in Figure 9. They were selected by GENESIS-PSI on the basis of SCR and temporal stability as measured by the amplitude dispersion index. A comparison with Figure 8 shows that their positions are strongly correlated with high SNR and SCR values. These PSs formed the reference network which was unwrapped using conventional PSI.

Wideband techniques that enable *detection of coherent scatterers from a single SSC* [14] were also investigated but these results will be published elsewhere.

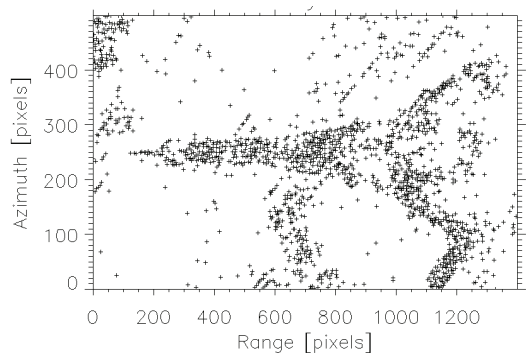

Figure 9. PSs selected by GENESIS-PSI within the RoI.

Conventional Processing

The result of conventional unwrapping shown in Figure 10 corresponds well to the actual height of the Eiffel tower of 324 m. The estimated standard deviations of the topography estimates lie mostly between 1–3 m. Errors do occur at points not on the Eiffel tower, namely points at upper left which are estimated to lie at an elevation of about 200 m (blue) with respect to the reference PS but actually lie nearer to ground level (orange). This is caused by arcs extending from the top of the Eiffel tower to the opposite bank – thus connecting PSs with no direct physical connection – and a lack of arcs which cross the river over physically connected structures such as bridges. The former arcs dominate the inversion process and pull points on the opposite bank up to the height at the tower's top. Processing over a larger RoI would ameliorate this effect. In such situations where spatial PU errors occur, pixelwise independent estimates provided by delta-k absolute phase estimation would be of use.

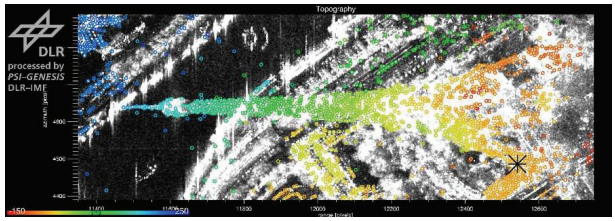

Figure 10. Topography from conventional PSI.

Error Sources

Possible sources of error in the delta-k absolute phase estimate were identified and their expected effect was determined. Effects considered included the hydrostatic, wet and liquid components of the atmosphere, the ionosphere and orbit error. Instrument and processing errors were found to be negligible in comparison. For the small region of interest around the Eiffel tower, the net effect was found to be a spatially invariant bias in the delta-k phase on the order of one cycle at the carrier frequency. Limited spatial inhomogeneity may arise due to the height of the Eiffel tower and the presence of liquid water and water vapour. In conventional PSI, a constant phase bias disappears as only the differential phase between the PSs and a reference PS is considered. The same is true for delta-k when the absolute phase estimates are referenced to the same PS.

Single Delta-k Interferogram Height Estimates

Single delta-k interferogram height estimates are obtained by simply scaling the delta-k phase with the HoA at the delta-k frequency. To avoid possible phase ambiguity, the HoA should be at least as large as the change in topography over the scene, preferably slightly larger to allow for some phase error. To make optimal

use of the available HoA, the reference point or reference surface used to calculate the FEP should then lie midway between the minimum and maximum heights over the scene. The required a priori knowledge is obtainable from an SRTM DEM. Although large HoAs are then advantageous in avoiding ambiguity with large changes in topography, they also lead to greater height errors because of the greater sensitivity to phase noise.

Figure 11 shows an example of this estimator where the delta-k HoA was ~1.1 km. Height estimates are with respect to a reference surface located 240 m above the WGS84 ellipsoid. The base of the Eiffel tower is located about 160 m below this reference surface. In comparison to the fullband interferometric phase, the standard deviation of the delta-k absolute phase is larger by a factor of $\sqrt{2}k_A \approx 68$ for the Paris acquisitions. This is the reason that most pixels within the RoI, especially those not on the Eiffel tower, appear very noisy with height estimates randomly distributed over ±HoA/2. In spite of this, the form of the Eiffel tower is clear and its height can be roughly determined.

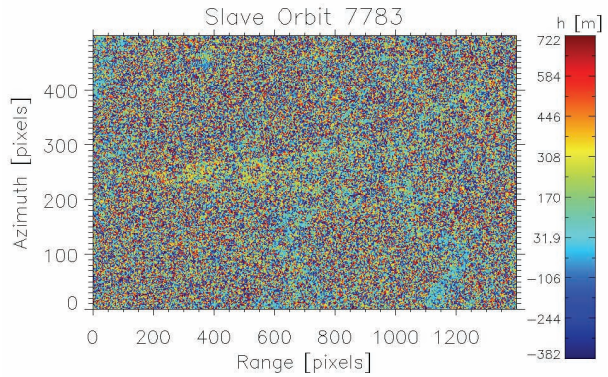

Figure 11. An example of single interferogram delta-k height estimation. The delta-k HoA was 1104 m.

For verification purposes only, Figure 12 shows the same example as in Figure 11 but with smoothing of the delta-k phase prior to scaling by the delta-k HoA. Smoothing was performed just as for DEM generation with a 3dB filter width of 50×50 pixels (slant range × azimuth) or 20×21 m (ground range × azimuth). Only pixels with an SNR greater than 25 dB are shown. The smoothing greatly reduces the noise and the height of the Eiffel tower is easily estimated to be ~300 m. The corresponding single look fullband interferometric phase with a HoA of 23 m is also shown. Visual unwrapping gives about 13 fringes running up the Eiffel tower for a height difference of 13×23 = 299 m.

Least Squares Delta-k Height Estimates

Since the delta-k phase is linearly proportional to height above the reference surface through the h2p (height to phase ratio), height estimates can be obtained from a LS

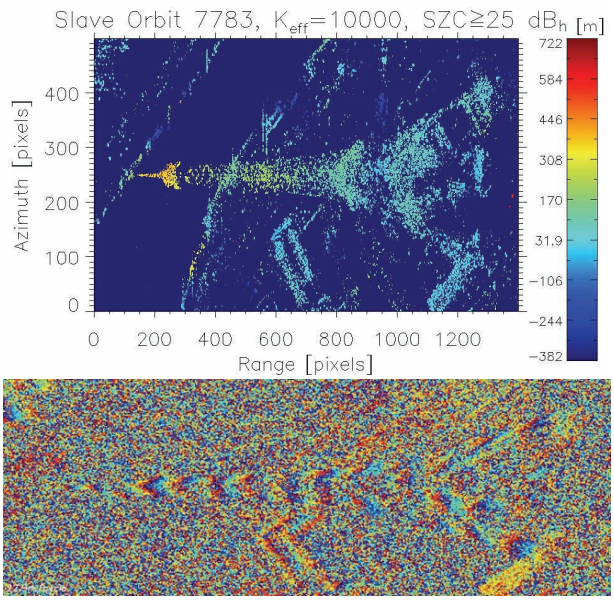

Figure 12. (Top) The same example as in Figure 11 but with smoothing of the delta-k phase and thresholding at an SNR of 25 dB. (Bottom) Corresponding fullband interferometric phase using 36 looks.

regression of the delta-k phase on the h2ps across all delta-k interferograms in the stack. This provides one height estimate per pixel per stack. To avoid breakdown due to phase error, the reference surface should be carefully chosen, just as discussed previously. Figure 13 shows this estimate where the reference surface was shifted to 240 m above the WGS84 ellipsoid. This shift was corrected for so that an estimated height of 0 m corresponds to the original reference surface at 70 m above the WGS84 ellipsoid. From a visual inspection, the base of the tower can be seen to lie at ~0–100 m with the top climbing to ~400 m.

It can be shown that the theoretical variance of this estimate is inversely proportional to the sum of squared h2ps. Hence the largest h2ps / normal baselines / smallest HoAs play the greatest role in reducing variance. Maximising the sum of squares of normal baselines with respect to the master orbit will then minimise estimator variance. This was done here.

The LS estimate ignores correlation across interferograms due to the use of a common master. Including this in the regression model gives a weighted LS estimator. Experiments have shown that this does not lead to any significant improvement.

The spatial resolution of the LS estimator is equal to that of the delta-k interferograms but there is no temporal resolution due to the linear regression model of a constant height over time. The regression model is easily amended to allow for a time varying deformation such as a sinusoidal model to account for seasonal variation. Theoretical analysis not given here revealed that the error in such deformation estimates is likely to be on the order of the deformation itself – thus *single PS*

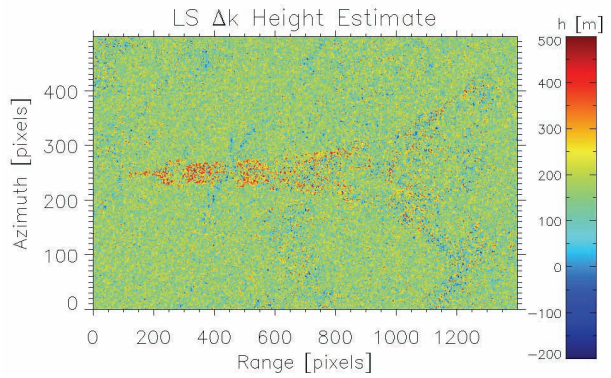

Figure 13. LS delta-k height estimates from a LS regression of the delta-k phase on the height to phase ratio over all delta-k interferograms.

deformation estimation using delta-k is not likely to be possible although *averaging over several PSs* may reveal deformation.

Comparisons

The major advantage of LS delta-k over single delta-k interferogram height estimation is that, aside from reduced variance due to a regression over the stack, errors due to the atmosphere, ionosphere and orbit error should average out over a large stack – even the spatially varying component due to atmospheric water vapour and liquid. For the single delta-k interferogram estimates, taking all estimates relative to a reference PS will cancel the spatially invariant component at the cost of error in the reference PS and, naturally, excluding the spatially varying error component. For both estimators, what will remain is a topography correlated spatial inhomogeneity due to elevation dependent atmospheric path delay.

To compare the conventional GENESIS-PSI and wideband LS delta-k height estimates an experiment was performed where for the 100 PSs with the smallest amplitude dispersion index over the Eiffel tower, relative height estimates were calculated using each PS in turn as a reference PS. The average RMS error between the wideband and conventional estimates was then found. The average RMS error was taken to be an estimate of the RMS error in the wideband estimate since the estimated average 1.9 m standard deviation of the conventional estimates was in relation so small that the conventional estimate could be assumed to approximate the true heights. This was considered a fair comparison because both conventional and wideband estimates make full use of the stack. The 147 m RMS error in the wideband estimates agrees well with that of the conventional estimate after scaling up by the factor $\sqrt{2}k_A \approx 68$ to account for the effect of subband differencing and the delta-k scaling factor giving $1.9 \times 68 \approx 130$ m. This shows that for strong PSs, the LS delta-k estimator reaches the limits of what it is capable of.

5. CONCLUSION

Delta-k absolute phase estimation promises to robustify PU for DEM generation, especially if custom chirps are used to increase the SNR. Its application to PSI is, at the moment, limited to all but the strongest PSs. However, as system bandwidths increase and SCRs decrease, delta-k for PSI will become more attractive.

6. REFERENCES

[1] R. Bamler and M. Eineder, "Accuracy of differential shift estimation by correlation and split-bandwidth interferometry for wideband and delta-k SAR systems," *IEEE Geoscience and Remote Sensing Letters*, vol. 2, no. 2, pp. 151–155, April 2005.

[2] R. Brcic, M. Eineder and R. Bamler, "Interferometric Absolute Phase Determination with TerraSAR-X Wideband SAR Data", 2009 IEEE Radar Conference, Pasadena, May 2009.

[3] R. M. Goldstein, H. A. Zebker, and C. L. Werner, "Satellite radar interferometry: Two-dimensional phase unwrapping," *Radio Sci.*, vol. 23, pp. 713–720, 1988.

[4] A. Ferretti, C. Prati and F. Rocca, "Permanent scatterers in SAR interferometry," *IEEE Trans. Geoscience and Remote Sensing*, vol. 39, no. 1, pp. 8-20, Jan. 2001.

[5] B. M. Kampes, *Radar Interferometry: Persistent Scatterer Technique*, Series: Remote Sensing and Digital Image Processing, vol. 12, Springer, 2006.

[6] S. N. Madsen, "On absolute phase determination techniques in SAR interferometry," Proceedings SPIE Conference on Radar Sensor Technology, vol. 2487, pp. 393–401, April 1995.

[7] M. Eineder and N. Adam, "A maximum-likelihood estimator to simultaneously unwrap, geocode, and fuse SAR interferograms from different viewing geometries into one digital elevation model," *IEEE Trans. Geoscience and Remote Sensing*, vol. 43, no. 1, pp. 24-35, Jan. 2005.

[8] C. Fischer, K. Schmitt and W. Wiesbeck, "3-D interferometric SAR algorithm for discontinuous distributed objects," IGARSS-99, Hamburg, Germany, June 1999.

[9] V. Pascazio, and G. Schirinzi, "Multifrequency InSAR height reconstruction through maximum likelihood estimation of local planes parameters," *IEEE Trans. Image Proc.*, vol. 11, no. 12, pp. 1478–1489, Dec. 2002.

[10] R. Scheiber and A. Moreira, "Coregistration of interferometric SAR images using spectral diversity," *IEEE Trans. Geoscience and Remote Sensing*, vol. 38, no. 5, pp. 2179–2191, Sep. 2000.

[11] N. Veneziani and V. M. Giacovazzo, "A multi-chromatic approach to SAR interferometry: Differential analysis of interferograms at close frequencies in the spatial domain and frequency domain," IGARSS-06, Denver, Colorado, USA, July 2006.

[12] W. Xu, E. C. Chang, L. L. Kwoh, H. Lim, and W. C. A. Heng, "Phase-unwrapping of SAR interferogram with multi-frequency or multi-baseline," IGARSS-94, pp. 730–732, Pasadena, California, 1994.

[13] R. Hanssen, *Radar Interferometry*. Kluwer Academic Publishers, 2001.

[14] R. Zandona-Schneider, K. P. Papathanassiou, I. Hajnsek, and A. Moreira, "Polarimetric and interferometric characterization of coherent scatterers in urban areas," *IEEE Trans. on Geoscience and Remote Sensing*, vol. 44, no. 4, pp. 971–984, April 2006.